ARTÍCULO DE INVESTIGACIÓN
Vol. 34, No. 2, Agosto 2013, pp. 145-155

Revista Mexicana de Ingeniería Biomédica

SOMIB

CAT and MRI Studies of Spinal Cord Injured Rats Implanted with PPy/I

A. Morales-Guadarrama*,**
H. Salgado-Ceballos****
J. Morales***
C. Ríos*****
G.J. Cruz******
A. Diaz-Ruiz*****
M.-G. Olayo******
L. Alvarez-Mejia*
R. Mondragón-Lozano*
R. Olayo***

*Departamento de Ingeniería Eléctrica, **CI3M, ***Departamento de Física. UAM-Iztapalapa. **** Centro Médico Nacional Siglo XXI México. ***** Instituto Nacional de Neurología y Neurocirugía Manuel Velasco Suárez. ******Departamento de Física, ININ
Correspondencia:
Roberto Olayo
Departamento de Física.
Universidad Autónoma Metropolitana Iztapalapa. Av. San Rafael Atlixco 186 Col. Vicentina Del. Iztapalapa, México D. F. CP. 09340
Correo electrónico:
oagr@xanum.uam.mx

Fecha de recepción:
31 de Octubre de 2012
Fecha de aceptación:
18 de Junio de 2013

ABSTRACT

Polymers synthesized by plasma derived from pyrrole have been recently implanted in rats with spinal cord injuries (SCI) using a complete section model; the polymers contribute to the functional recovery after the injury. In this work, the SCI in rats was studied using noninvasive techniques such as magnetic resonance imaging (MRI). Also computerized axial tomography taken chronologically with and without polymeric implants. 3D reconstructions were used to follow the structural arrangement, the location of the implant and the formation of cysts. MRI shows a clear differentiation between white and gray matter, the implanted material and cysts due to secondary damage after the injury.

Keywords: spinal cord injury recovery, MRI, CAT, plasma synthesis.

RESUMEN

Polímeros sintetizados por plasma derivados del pirrol, han sido implantados en ratas con lesión de médula espinal (LME) usando un modelo de lesión por sección completa; los polímeros contribuyen a la recuperación funcional después de la lesión. En este trabajo, la LME se estudió usando técnicas no invasivas como imágenes por resonancia magnética (IRM) y tomografía axial computarizada tomada cronológicamente en sujetos con y sin implante polimérico. Se usaron reconstrucciones 3D para seguir el arreglo estructural, la localización del implante y la formación de quistes. Las IRM muestran una clara diferenciación entre materia gris, materia blanca, material implantado y quistes formados debido a los mecanismos de daño secundario después de la lesión.

Palabras clave: recuperación de lesión de médula espinal, IRM, TAC, síntesis por plasma, pirrol.

INTRODUCTION

The spinal cord is responsible for transmitting signals to and from the brain. However, after a spinal cord injury (SCI), the motor and sensorial functions are substantially reduced, and no effective therapeutic strategies to restore the normal nerve functions have been developed. This problem is worsened due to the complexity of regulating mechanisms of secondary damage and to the low capacity of spontaneous neuronal cell regeneration.

The possible benefits of implants in the nervous tissues after a SCI to promote functional recovery have been discussed for many years, because the implants could stimulate some growing factors. Various protocols have been developed: cell cultures [1, 2], embryonic neural stem cells [3, 4], neuroprotection [5, 6], rehabilitation [7, 8], etc. These studies have shown that implants promote significant functional recovery, however, their mechanisms are still unclear. In this trend, conducting polymers synthesized by plasma implanted in adult rats with complete spinal cord transection have favored the protection of the nervous tissue adjacent to the lesion and significantly increased the functional recovery of animals, when compared with injured animals without implants [9, 10].

The degree of initial damage and pathobiological events subsequent to the injury are usually evaluated using invasive or terminal methods based in histology or immunohistochemistry to correlate with the motor or sensorial functions in SCI models. Although these traditional methods are essential to establish the ways and mechanisms involved in post-injury events, it is necessary to sacrifice animals at different stages to obtain tissue for the histological evidence. On the other hand, in vivo approaches, such as computerized axial tomography (CAT) and magnetic resonance imaging (MRI) provide a way to follow the evolution of the lesion in a noninvasive manner preserving the life of the animals for longer periods [11, 12].

MATERIALS AND METHODS

Material Synthesis and Characterization

Pyrrole and iodine used in the synthesis and the solvents applied to remove the polymers were purchased from Sigma-Aldrich and used without further purification. Once the PPy/I films were synthesized, acetone was applied to separate the films from the substrates and to dissolve the remaining oligomers. The film was left in the reactor for 24 hr. In an iodine atmosphere to neutralize the last free radicals and to increase the amount of iodine in the polymers.

The PPy/I films were pulverized in an agate mortar to obtain a fine brown powder, which was compressed at 9 tons for 10 min to form a thin tablet, which was implanted in the rats. FT-IR, TGA, and morphological analyses were performed on the polymers before the compression. The electrical conductivity was calculated from the resistance measured directly from the tablet.

Electrical Properties

The electrical resistance of PPy/I was measured with a digital OTTO MX620 multimeter in a capacitive arrangement with the polymer between two copper electrodes. The electrical conductivity of the tablet was calculated using the following equation:

$$\sigma = \frac{1}{\rho} = \frac{L}{RA}$$

Where R, ρ and σ are the resistance, resistivity and electrical conductivity respectively. L is the tablet thickness and A is the cross-section area. The PPy/I presents a resistance of 1.3 MΩ at 25% of relative humidity, a resistivity of 45.94 MΩ cm, and an electrical conductivity of 21 nS/cm.

Injury model and implantation

This study followed the guidelines established in the regulations of the General Health Law for research in health in Mexico. 16 adult female Long Evans rats were used; 12-14 weeks age with

body weight between 230-250 g. The rats were divided in 2 groups:

- Control Group. 8 rats, which underwent a spinal cord transection at the 9th thoracic vertebra (T9).
- PPy/I Group. 8 rats with spinal cord transection but implanted with a PPy/I tablet in the lesion site.

To perform spinal cord transection, the animals were anesthetized intramuscularly with a mixture of ketamine and xylazine hydrochloride, 77.5 mg and 12.5 mg respectively, per kg of body weight. A sagittal incision was done followed by a dissection of the spine paravertebral muscles. Two spinous processes were removed, T8 and T9, and a 2-level laminectomy was made, extending bilaterally to facet processes. The meninges were kept intact. A longitudinal incision in the meninges of about 5 mm long was applied referencing both sides of the incision with a simple point of suture 10-0 (Polypropylene knatel©). After that, the spinal cord was transected, microsurgery hook and surgical microscope were used to corroborate that no nerve pathways were connected.

Immediately after the injury, a piece of 3 mm diameter PPy/I tablet was implanted in the specimens of the PPy/I group. Both groups were sutured with 10-0 suture through the meninges with stitches. Finally, the surgical incision was sutured in 2 planes, the muscle fascia and skin.

Computerized axial tomography

For the computerized axial tomography study an Elscint Tomograph model CT-TWIN was used. The main parameters were field of view (180 mm), current density (50-500mAs) and, potential (120 kV); with a 0.2 mm slice. In order to study the integration of the material in the spinal cord tissue, tomographic sessions were performed, one each week after the injury. To find the best possible operating parameters of the tomograph, different tests were performed. Figure 1 shows 3 runs with different operating parameters.

The first study (Figure 1A) has images of 180 mm, 50 mAs and 120 kV. The contrast of the implanted material was good but the soft tissue contrast shows apparent small voids that may generate confusion with the cysts formation in the spinal cord.

The next image was taken with the following parameters: 180 mm, 300 mAs, and 120 kV obtaining a small contrast difference in soft tissue, this makes difficult the interpretation of images in the spinal cord (Figure 1B).

The best parameters in the studies (Figure 1C) were: 180 mm, 500 mAs and 120 kV. With these values, a higher resolution was achieved in soft tissue and voids, although the material-bone contrast was compromised. This was later used to analyze the spinal cord evolution enhancing the contrast with false color.

Magnetic Resonance Image

MRI studies were performed in a Varian 7T instrument, using standard gradient echo sequence with the following acquisition parameters: TE/TR = 4/15ms, FOV = 60 × 60mm, angle = 20°, matrix size = 256×256, NEX = 6. Figure 2 shows images obtained outside the area of injury, at the top center of the Figure 2 the intact cytoarchitecture of the nerve tissue can be observed, where the main feature is the “H” shape of the white matter, surrounded by the vertebral disc in black. Figure 2 shows a close up of this structure.

An animal belonging to the PPy/I group with 4 weeks of recovery was chosen to extract a sample of spinal cord of 6.3 mm in diameter and 2 cm in length with reference to the implant (the

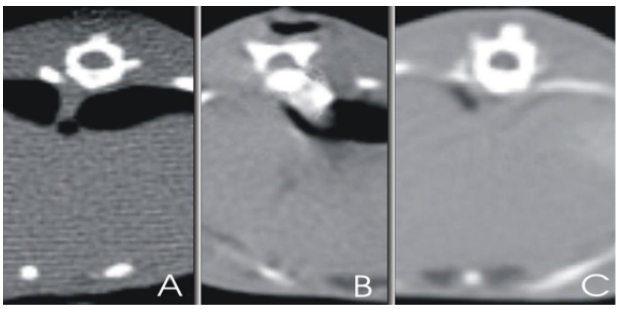

Figure 1. Tomographic slices with different parameters before to SCI: A) with 50 mAs, B) with 300 mAs, C) with 500 mAs.

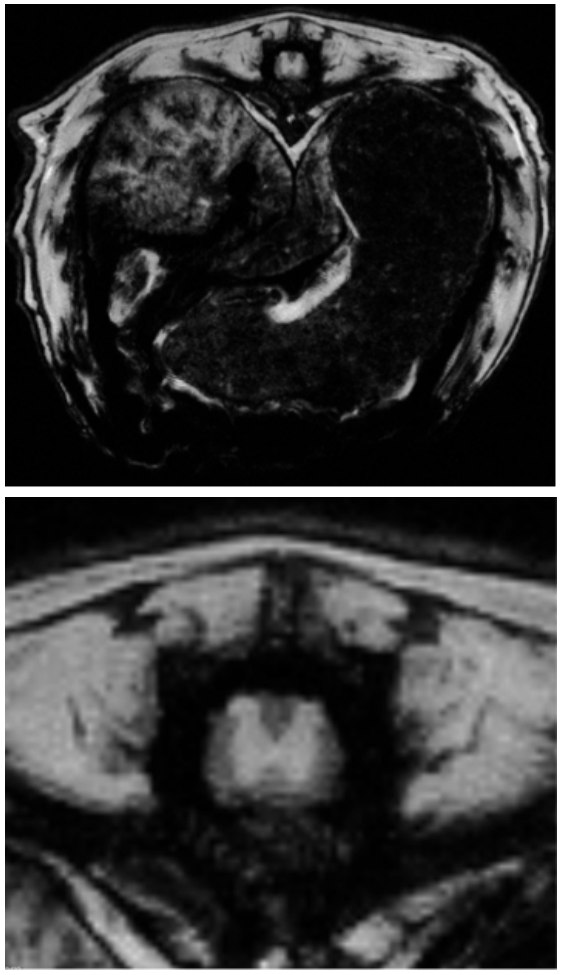

a)

b)

Figure 2. A) MRI obtained with GEMS sequence; B) Image showing the spinal cord area.

Figure 3. MRI obtained with GEMS sequence of the insolated spinal cord.

injury epicenter) and was placed in an acrylic container with 10% formaldehyde. A magnetic resonance imaging study was performed to this sample. Gradient echo sequences were used with the following acquisition parameters: TE/TR = 5/20ms, FOV = 20x20mm, angle = 20°, matrix size = 128 × 128, NEX = 10. The studies were obtained with DICOM format (Figure 3).

Sacrifice and histology

The animals were anesthetized with a mixture of 12.5 mg 77.5 mg of ketamine hydrochloride and xylazine by kg/body-weight, and perfused intracardially with 200 ml of saline with 1000 u.i Heparin, followed by 500 ml of formaldehyde (10%). Both solutions were transfused at a rate of 30 ml/min with a peristaltic pump. After the perfusion, the spinal cord was removed to obtain a spanned segment of approximately 2 cm with the lesion epicenter in the middle. 10 μm thick sequential longitudinal cuts were made with a microtome, 10 samples were obtained (Figure 4). The segments were transferred to a water bath at 45°C (each liter of water had 0.5 g of bacteriological gelatin) and then placed on glass slides to be stained with the hematoxylin-eosin procedure.

RESULTS AND DISCUSSION

Computerized axial tomography

The CAT studies were done with the OSIRIX-software using a DICOM (Digital Imaging and Communications in Medicine) format. The absorption coefficient was evaluated, with the Hounsfield scale; it gives +1000 for bones, 0 for water and -1000 for air. The PPy/I coefficient was 100 ± 20, the value of nerve tissues are between 22 and 46 (gray matter 22-32 and white matter 36-46).

The segments of interest in the images were highlighted by applying a stain (false color) in the range of the Hounsfield scale enhancing the contrast between nerve tissues and bones. This effect can be seen in Figure 5, where the vertebral disc is in white and the spinal cord has two colors associated with the spinal cord tissue.

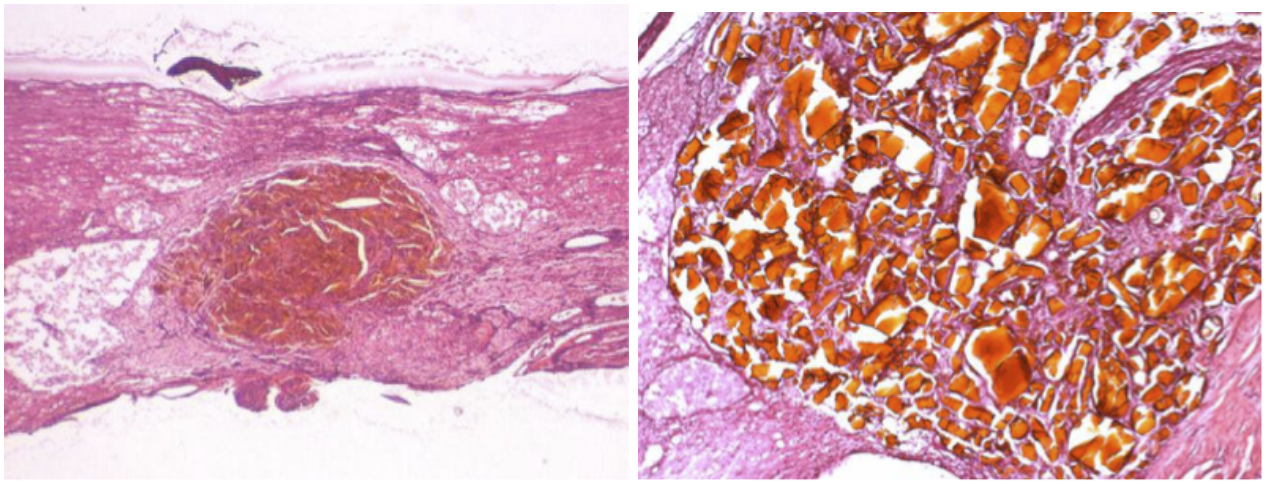

Figure 4. Histology of spinal cord with PPy/I implant shows the integration of the implant with nerve tissue.

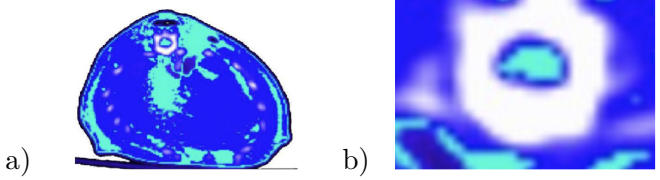

Figure 5. a) Slice for subject without implant; b) Enlargement: vertebral disc and nerve tissue.

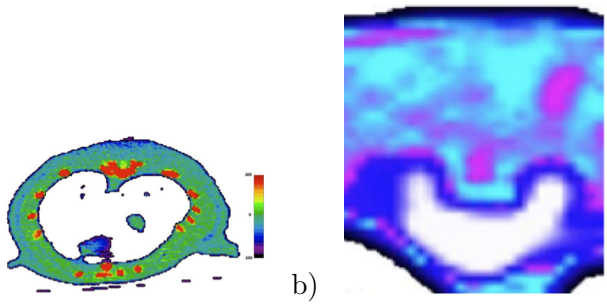

Figure 6. Interval of colors applied to the images.

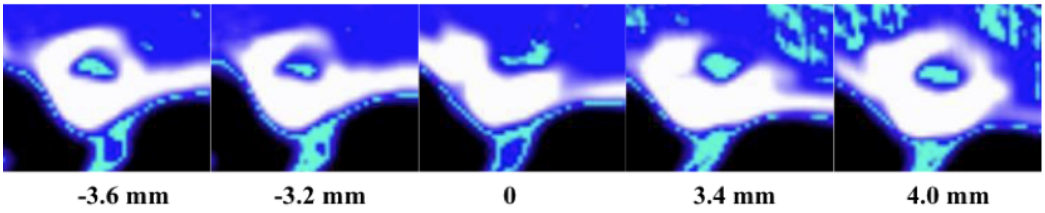

Figure 7. Epicenter injury slices.

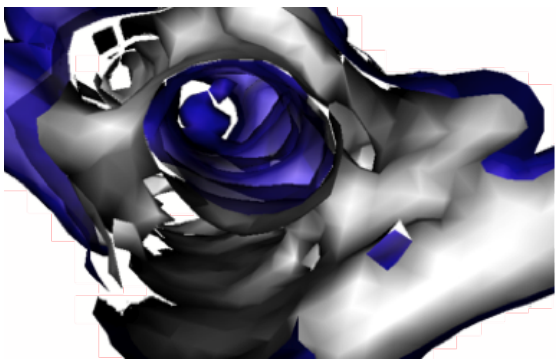

Figure 8. 3D reconstruction with implant polymer (center).

Figure 6 shows the color scale associated to the Hounsfield scale, to illustrate how it is possible to identify different tissues or materials as the implant. In the close-up, it is possible to observe the bone, spinal cord and implant material, the white zone is the bone (the dissected vertebral disc) and inside it the nerve tissue surrounds the implant material (almost square).

The CAT study consisted of different sequences of slices taken in a specific axis in the lesion zone with a 0.2 mm gap between each

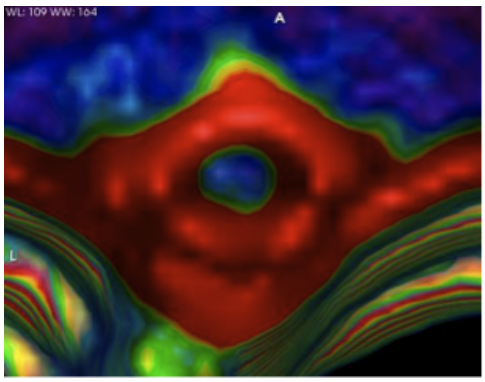

Figure 9. Colored image before the laminectomy zone with preserved tissue.

slice. Figure 7 shows the slices obtained from an animal in the control group 5 weeks after the surgery. The normal nerve tissue and vertebral disc can be seen in the 4 mm image. The epicenter of the lesion is located at 0 mm, which shows no spinous process and a patch cord tissue disintegrated. The images located at -3.6 mm and -3.2 mm shows the laminectomy partially.

CAT 3-D reconstructions

The tomographic images of the injured rats were reconstructed in 3D sequences with OSIRIX to follow the implant position, the laminectomy, the presence of cysts and the nerve tissue preservation. Figure 8 shows a recreation formed with 10 slices taken with a 180 mm field vision, current density of 300 mAs and a potential of 120 kV. The distance between each slice is 1 mm, the vertebral canal is showed and at the center the semi-square piece of implanted material can be observed.

Figure 9 shows an image of a non-injured segment of the spinal cord discerning the vertebral disc and the spinal cord, which is located in the center.

CAT and histology

Control and implanted groups of rats have significant histological differences. Figure 10 shows that the PPy/I group has the implant integrated in the spinal cord with a great preservation of the cytoarchitecture. Nerve cells can be seen around some fragments of PPy/I. It is even possible to follow paths of cells suggesting a connection of the spinal cord through the implant. In the control group, a barrier of large cysts appears at the sides of the lesion with an extensive destruction of the medullar cytoarchitecture. This may block the communication in the zone.

Figure 11 contains 2 images of the lesion zone after 8 weeks. In the PPy/I group, the implant has moved partially from the original site by the histological cuts, leaving voids of different size behind. This is due to the fragmentation of the tablet by the tissue growth. In the Control group, the cysts are much bigger than in the PPy/I group suggesting coalescence of cysts. The histological images show that the implant affects the evolution of the tissues after the lesion.

Figure 12 contains two 3D reconstructed images of the injured area. The left image corresponds to a rat implanted with PPy/I, 4 hr. after the surgical procedure. The polymeric implant is located in the central part of the spinal canal, in the spinal cord. The right figure shows an image of the same animal taken 4 weeks after the injury, where it is possible to observe some disaggregation of the implant. The absence of the corresponding spinous processes delimits the lesion area.

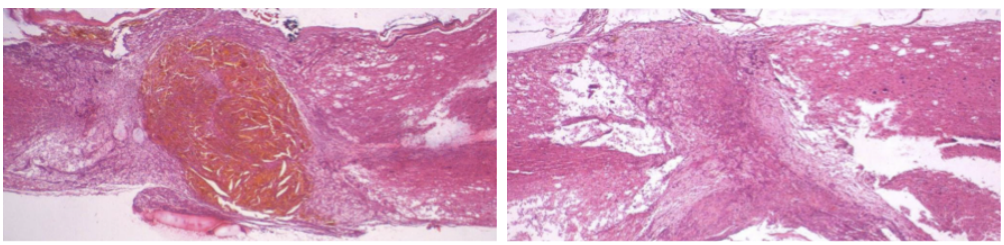

Figure 10. Histological images, first week, PPy/I (left) and control groups (right).

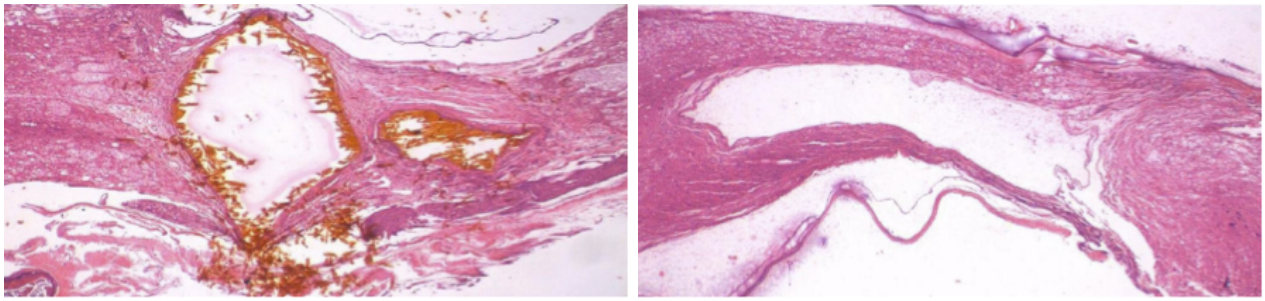

Figure 11. Histology eight weeks after the injury, both groups PPy/I (left) and Control (right).

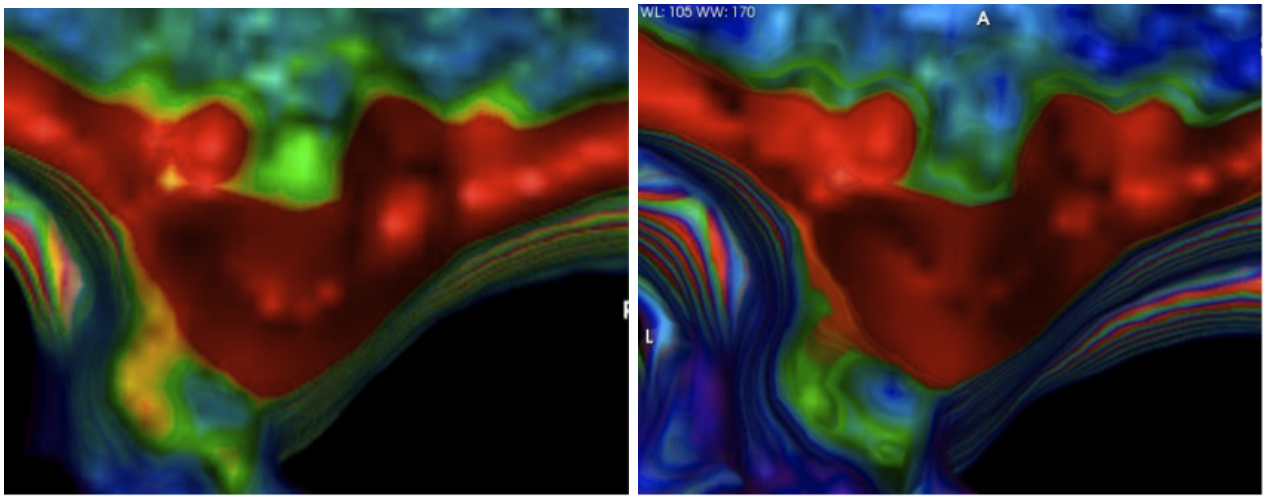

Figure 12. PPy/l implant. Left 4 hr. post-injury, and right 4 weeks.

Magnetic Resonance Image

The MRI studies were processed with OSIRIX using a DICOM format. Figure 13 shows images extracted from a 3D reconstruction (The full video is available on demand from the authors). Figure 13 A) shows post processing 7T study, inches away from the epicenter of injury. Figure 13 B) close up of the spinal cord area, which shows the conserved cytoarchitecture, the H-shaped gray matter is clearly defined. The ROI (oval between the dorsal horns) is positioned on the cephalic side of the lesion. Figure 13 C) Axial section at the epicenter of the lesion, we observe the destruction of cytoarchitecture.

The arrow indicates the ROI in the caudal side of the lesion. The other ROIs delineate the area of injury. In Figure 13 D) shows a coronal section of the epicenter of the injury, surviving gray matter can be seen (hyperintense area) on the sides of the zone of injury. A sagittal view in the middle of the spinal cord is shown in Figure 13 E) it shows the lesion extension.

In the dissected spinal cord MRI, we obtained a resolution of 156 μm pp, Figure 14 A) shows the reconstruction of these MRI, with the center at the epicenter of injury. The axial section B) highlights the gray matter (hyperintense signal), the ventral root filaments at both ends at the base of the spinal cord (also hyperintense signal), we observe the meninges covering the spinal cord. In both, between the dorsal horns (center) and along the lateral horns, shows the extent of the lesion (hypointense signal) in the cephalic region. Selected view of the injury area shows a scattered gray and white matter; indicating that the morphology and cytoarchitecture of the spinal cord was destroyed, C) the implant and surrounding contrasting tissues suggest some preserved gray matter. D) Shows a waist in the spinal cord, characteristic of the lesion and the implant partially fused with the surrounding tissues. The resolution obtained allows us to observe tissue growth through the implant (arrow) in the lesion epicenter.

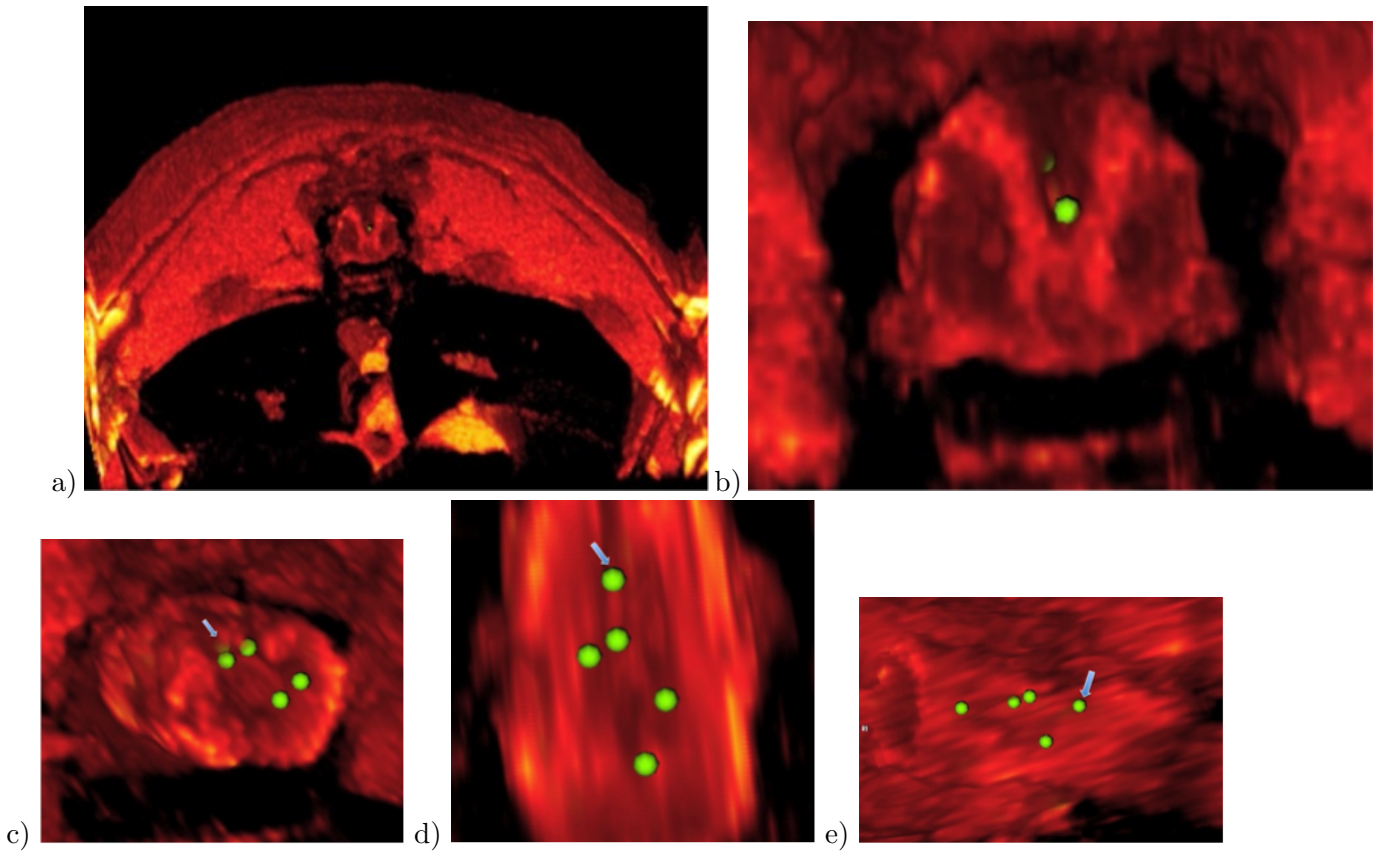

Figure 13. A) Post Processed IRM. B) Closeup of the spinal cord area. C) Axial View at the epicenter of the lesion. D) Coronal section of the lesion. E) Sagittal view in the middle of the spinal cord.

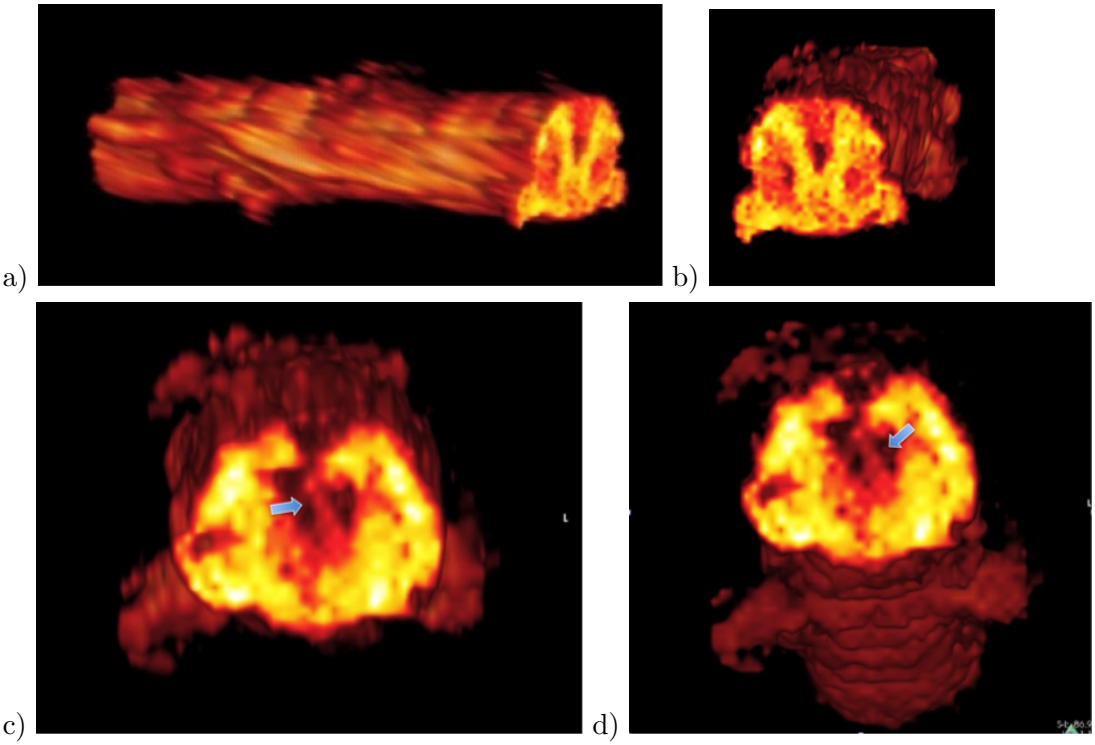

Figure 14. A) Dissected spinal cord MRI Reconstruction. B) Axial section, cephalic area of the lesion. C), D) Axial section of the injury epicenter, the arrow points to tissue growth through the implant.

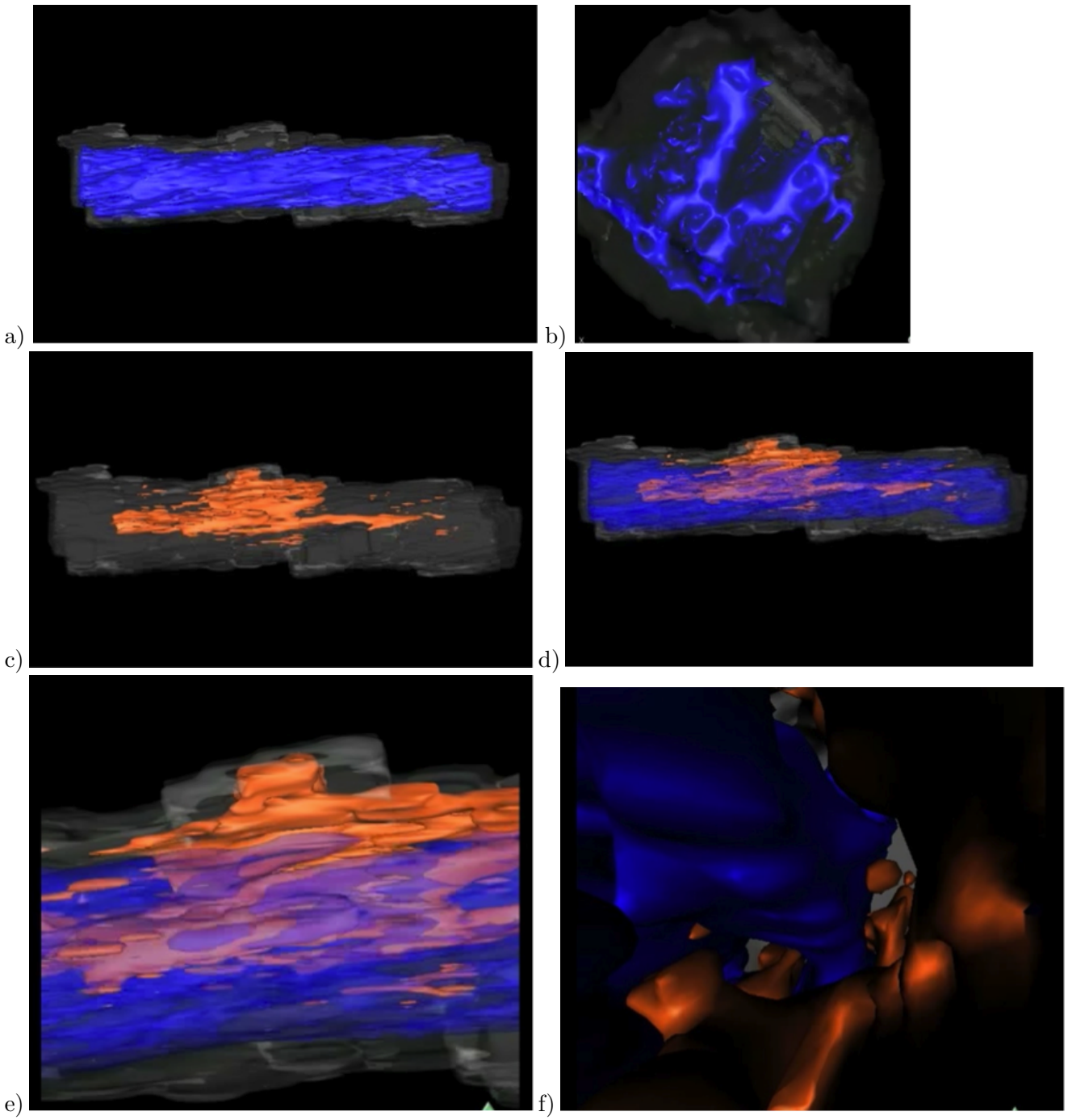

Figure 15. Processing focused on surfaces. A) Gray Matter. B) Gray Matter. C) Material, Cysts or voids. D) and E) Fusion between Gray Matter, Material, Cysts and voids. F) Internal view showing the growth of gray matter.

Processing focused on the surface of the gray matter shown in Figure 15 A) shows the continuity of the tissue through the entire sample. Figure 15 B) shows the axial view of this processing, which enhances the morphology of the gray matter. The Figure 15 C) focuses on the signal that corresponds to the material, cysts or voids in the sample. One can observe the material displaced towards the dorsum of the subject, this due to mechanical forces by tissue ingrowth. The fused images of gray matter and material are showing in Figure 15 D). In both, Figure 15 D) and Figure 15 E) shows the presence of gray matter through the implant

(arrow). Figure 15) is an internal view showing the growth of gray matter in the epicenter of the injury, through the implant.

CONCLUSIONS

Computed tomography and magnetic resonance imaging were used in this work to follow the progress of the injury zone in a total spinal cord transection *in vivo* model of rats with spatial resolution of tenths of millimeter. The images were contrast enhanced with color and represented in 3D reconstructions, which allowed differentiating the fragmentation of the implant, the different damaged zones of the spinal cord and the existence of cysts. The Computed tomography is limited by the spatial resolution, however, the contrast between bone and tissue facilitated the location of the implant. The magnetic resonance images provided greater resolution than computed axial tomography and with this technique the implant fragmentation, the formation of cysts around the area of injury and the proliferation of tissue throughout the implant could be observed.

In vivo approaches, such as computerized axial tomography and magnetic resonance imaging provide a way to follow the evolution of the lesion and the characterization of this implanting therapy in a noninvasive manner preserving the life of the experimental subjects for longer periods.

ACKNOWLEDGEMENTS

The authors wish to thank CONACyT and ICyT-DF for the financial support to this work under the projects CONACyT-155239, ICyT-DF- PIUTE 10-63, 276/2010 and ICyT-DF-PICSA11-14/2011.

REFERENCES

1. Bianco J.I., Perry C., Harkin D.G., Mackay-Sim A., Feron. (2004) "Neurotrophin promotes purification and proliferation of olfactory ensheathing cells from human nose." Glia 45: 111-123.

2. Lu J., Feron F., Mackay-Sim A., Waite, P.M. (2002) "Olfactory ensheathing cells promote locomotor recovery after delayed transplantation into transected spinal cord." Brain 125: 14:20.

3. Thompson F.J., Reier P.J., Uthman B., Mott S., Fessler R.G., Behrman A., Trimble M., Anderson D.K., Wirth III E.D. (2001) "Neurophysiological assessment of the feasibility and safety of neural tissue transplantation in patients with syringomyelia." J. Neurotrauma 18: 931-945.

4. Keirstead H.S., Nistor G., Bernal G., Totoiu M., Cloutier F., Sharp K., Steward O. (2005) "Human embryonic stem cellderived oligodendrocyte progenitor cell transplants remyelinate and restore locomotion after spinal cord injury." J. Neurosci. 25: 4694-4705.

5. Baptiste, D. C., Fehlings, M. G. (2006) "Pharmacological approaches to repair the injured spinal cord." J. Neurotrauma 23:318-334.

6. Hall, E. D., Springer, J. E. (2004) "Neuroprotection and acute spinal cord injury: a reappraisal." NeuroRx 1:80-100.

7. Kwon B.K., Liu J., Oschipok L., Teh J., Liu Z.W., Tetzlaff W. (2004) "Rubrospinal neurons fail to respond to brain-derived neurotrophic factor applied to the spinal cord injury site 2 months after cervical axotomy." Exp. Neurol. 189:45-57.

8. Engesser-Cesar C., Anderson A.J., Basso D.M., Edgerton V.R., Cotman C.W. (2005) "Voluntary wheel running improves recovery from a moderate spinal cord injury." J. Neurotrauma 22:157-171.

9. Olayo R., Ríos C., Salgado-Ceballos H., Cruz G., Morales J., Olayo G., Alvarez L., Mondragón R, Morales-Guadarrama A., Guizar-Sahagun G., Diaz-Ruiz A. (2008) "Tissue spinal cord response in rats after implants of polypyrrole and polyethylene glicol obtained by plasma." Journal of

Materials Science; Materials in Medicine 19(2):817-826.

10. Cruz G.J., Mondragón-Lozano R., Diaz-Ruiz A., Manjarrez J., Olayo R., Salgado-Ceballos H., Olayo M.G., Morales J., Alvarez-Mejía L., Morales A., Méndez-Armenta M., Plascencia N., Fernandez M., Ríos C. (2012) "Plasma polypyrrole implants recover motor function in rats after spinal cord transection." J Mater Sci: Mater Med 28:2583-2592.

11. Bilgen M, Al-Hafez B, Alrefae T, He YY, Smirnova IV, Aldur MM, Festoff BW. (2007) "Longitudinal magnetic resonance imaging of spinal cord injury in mouse: changes in signal patterns associated with the inflammatory response Jun." Magn Reson Imaging. 25(5):657-64.

12. Gonzalez-Lara LE, Xu X, Hofstetrova K, Pniak A, Brown A, Foster PJ. (2009) "*In vivo* magnetic resonance imaging of spinal cord injury in the mouse." J Neurotrauma. 26(5):753-62.